Molecular Dynamics Study of the Thermodynamic Properties of Calcium Apatites. 2. Monoclinic Phases

Fernando J. A. L. Cruz, José N. Canongia Lopes, and Jorge C. G. Calado*

Centro de Química Estrutural, Complexo Interdisciplinar, Instituto Superior Técnico, 1049-001 Lisboa, Portugal

Received: October 11, 2005; In Final Form: January 3, 2006

Structural and thermodynamic properties of crystalline monoclinic calcium apatites, $Ca_{10}(PO_4)_6(X)_2$ (X = OH, Cl), were investigated for the first time using a molecular dynamics (MD) technique under a wide range of temperature and pressure conditions. The accuracy of the model at room temperature and atmospheric pressure was checked against crystal structural data, yielding maximum deviations of ca. 2%. The standard molar lattice enthalpy ($\Delta_{lat}H^{\circ}_{298}$) of the apatites was also calculated and compared with previously published experimental and MD results for the hexagonal polymorphs. High-temperature simulation runs were used to estimate the isobaric thermal expansivity coefficient and study the behavior of the crystal structure under heating. The heat capacity at constant pressure, C_p, in the range 298−1298 K, was estimated from the plot of the molar enthalpy of the crystal as a function of temperature, $H_m = (H_{m,298} - 298C_{p,m}) + C_{p,m}T$, yielding $C_{p,m} = 635 \pm 7$ J·mol^{-1}·K^{-1} and $C_{p,m} = 608 \pm 14$ J·mol^{-1}·K^{-1} for hydroxy- and chlorapatite, respectively. High-pressure MD experiments, in the 0.5−75 kbar range, were performed to estimate the isothermal compressibility. The Parsafar−Mason equation of state was successfully used to fit the high-pressure $p-V_m$ data, with an accuracy better than 0.03%.

1. Introduction

In a previous work,[1] hereafter called Calcium Apatites-I, we have presented calculations for hexagonal calcium apatites, hydroxyapatite (HOAp), fluorapatite (FAp), chlorapatite (ClAp), and bromapatite (BrAp), obtained by the molecular dynamics (MD) technique. Thermodynamic properties such as the standard molar lattice enthalpy, $\Delta_{lat}H^{\circ}_{298}$, heat capacity at constant pressure, C_p, the pressure coefficient of the reduced volume, and the polynomial constants of an isothermal equation of state (EoS) have been estimated, and the results have been interpreted in terms of structural properties and potential energies. The compounds were modeled as hexagonal phases ($P6_3/m$) and could be well described by an all-atom Born−Huggins−Mayer (BHM) potential energy function.

It is known that both hydroxy- and chlorapatite can exist in two polymorphic phases:[2] hexagonal ($P6_3/m$) and monoclinic[3−5] ($P2_1/b$). The latter are sometimes referred to as "pseudohexagonal" apatites, for the corresponding structures arise from a distortion of the pure hexagonal forms and therefore exhibit a lower symmetry. In both polymorphs, the constituent ions present similar structural positions, the major difference being that the unit cell lengths change from (a, $b = a$, c) to (a, $b = 2a$, c), when going from the hexagonal to the monoclinic polymorph. Suda et al.[6] heated a monoclinic HOAp and verified that the X-ray diffraction (XRD) characteristic lines of the monoclinic form begin to disappear at 473 K, decreasing further until they are no longer present in the diffractogram; beyond 483 K, the XRD profile of the sample corresponds to a $P6_3/m$ symmetry. On cooling the sample, the same authors found the transition to be reversible and of the λ-type and estimated the corresponding transition enthalpy and entropy as $\Delta H_{trans} = 630 \pm 25$ J·mol^{-1} and $\Delta S_{trans} = 1.30 \pm 0.05$ J·mol^{-1}·K^{-1}. Recently, Takahashi et al.[7] confirmed the occurrence and reversibility of such a transition by differential calorimetry. The same structural phenomenon in ClAp had been investigated earlier by Prener,[8] who estimated the transition temperature to be located at $T \approx 473$ K. Recently, Hochrein et al.[9] employed the MD technique to study the phase transition between monoclinic and hexagonal hydroxyapatite, found to be of an order−disorder type, with an activation energy of 50 kJ·mol^{-1}. However, they were only able to study the transition by running MD simulations for at least 730 ps (which in some cases had to be extended to 3 ns), to approach convergence. The process is therefore governed by very slow kinetics.

In pure hexagonal hydroxyapatite, all the OH^- anions are preferentially ordered along the crystallographic c direction.[10] The location and direction of the OH^- anions inside each "hexagonal" channel (see Figure 1a), defined as in Calcium Apatites-I, are similar in both polymorphic phases, but they are not the same throughout the entire solid structure in the monoclinic form. In the latter, the direction along which a column of OH^- ions is located is reversed when changing to an adjacent column. This can be visualized in Figure 1b.

In the past, little attention has been paid to the monoclinic phases of HOAp and ClAp, and therefore, the purpose of this work is to study those phases using MD simulations to estimate some of their relevant thermodynamic properties. Moreover, as far as we are aware, no MD simulations have ever been carried out for monoclinic chlorapatite. As in Calcium Apatites-I, we will start by calculating the cohesive energy of the monoclinic phases of hydroxy- and chlorapatite at room temperature ($T =$ 298 K) and atmospheric pressure ($p = 1$ bar), assuming the Born model for ionic solids.[11] The data will be compared with the experimental results obtained for the hexagonal phases,[1,12] as well as with simulation results.[1] High-temperature runs (298 K < T < 1298 K) have been used to estimate the heat capacity

* E-mail: jcalado@ist.utl.pt.

10.1021/jp055808q CCC: $33.50
Published on Web 02/04/2006

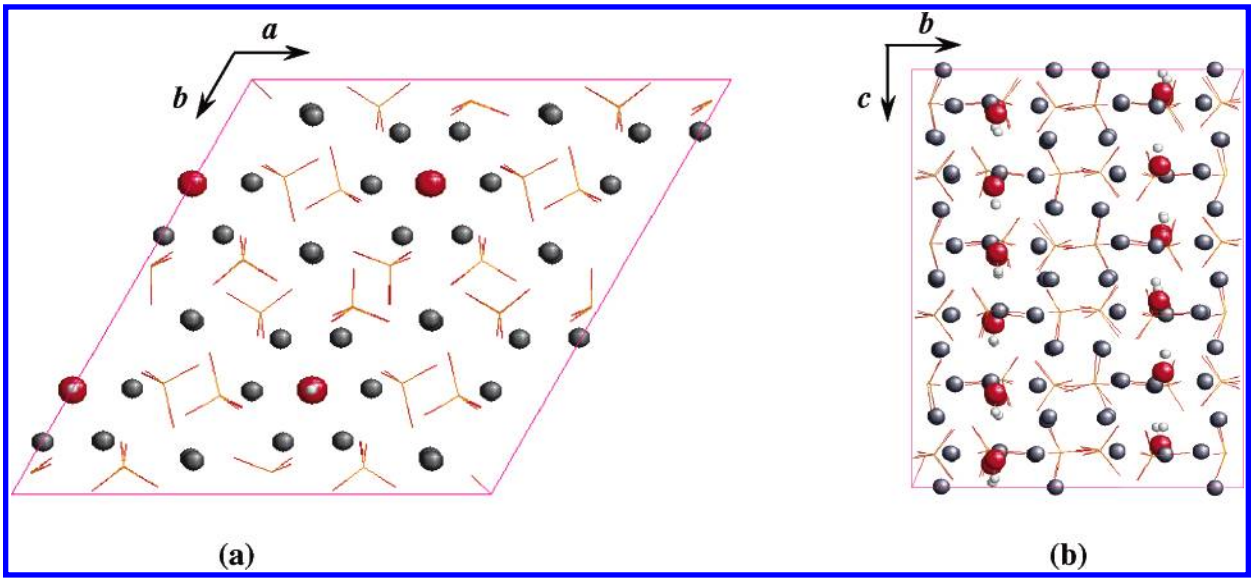

Figure 1. Snapshots of the 2 × 1 × 3 supercell of monoclinic hydroxyapatite: (a) *ab*-plane view, evidencing the pseudohexagonal symmetry around the hydroxyl anion and (b) side view along the crystallographic *c*-axis. Ca^{2+} = gray circles, O (H) = red circles, H = white circles, PO_4^{3-} = wireframe structure (3D rotatable images in *xyz* format are available for monoclinic hydroxy- and chlorapatite 2 × 1 × 3 supercells).

TABLE 1: Born−Huggins−Mayer Potential Energy Parameters (Equation 1)

	q_i	A_{ii} (kJ·mol^{-1})	B_{ii} (Å^{-1})	σ_{ii} (Å)	C_{ii} (kJ· Å^6·mol^{-1})
Ca	2	11.132	6.250	2.600	8.8928×10^2
P	2.6	20.873	3.333	3.400	2.8139×10^4
O (P)	−1.4	18.786	3.704	2.600	3.1266×10^3
O (H)	−1.6	15.446	4.505	2.600	1.3895×10^3
H	0.6	1.3916	50.000	0.200	1.3552×10^{-3}
Cl	−1	15.268	3.087	3.170	7.4384×10^3

at constant pressure, C_p, and the isobaric thermal expansivity coefficient, α_p. Given the energy values involved, the simulations do not have enough accuracy to reveal the solid-phase transition at 473 K. High-pressure simulation runs ($0.5 < p <$ 75 kbar) have been employed to obtain the isothermal compressibility, κ_T. The high-pressure results have been fitted and interpreted according to several equations of state (EoSs), namely, those of Tait,[13] Birch-Murnaghan,[14] and Parsafar and Mason.[15]

2. Experimental Section

Force Field Model. The all-atom force field used in the simulation runs to calculate the potential energy has already been described in Calcium Apatites-I and was recently also used by Hochrein et al. to study the transition between monoclinic and hexagonal hydroxyapatite.[9] It consists of a four-parameter Born−Huggins−Mayer potential energy function (BHM), as given by eq 1. The corresponding single atom parameters are given in Table 1.

$$U_{ij}(r_{ij}) = \frac{q_i q_j}{r_{ij}} + A_{ij}\exp[B_{ij}(\sigma_{ij} - r_{ij})] - \frac{C_{ij}}{r_{ij}^6} \qquad (1)$$

Variables and parameters have the usual meaning: r_{ij} is the distance between atoms *i* and *j*, C_{ij} is a measure of the dispersive energy, and the exponential term (A_{ij}, B_{ij}, and σ_{ij}) stands for the overlap of the electronic layers in ionic solids. The force field parameters for calcium, phosphate, and hydroxyl ions were taken from the work of Hauptmann and co-workers,[16] who used a rigid phosphate model for HOAp. For the repulsive term of the chloride anion, the results of Tosi and Fumi[17] have been used, while the data of Mayer[18] have been chosen to describe its dispersive energy.

Molecular Geometry and Simulation Details. The unit cell parameters of ClAp and HOAp have been determined, by single-crystal XRD, by Mackie et al.[3] and Elliott et al.,[4] respectively. In the present study, the atomic positions were generated applying the symmetry operations characteristic of the ($P2_1/b$) space group[19] to the solid-state XRD data. The unit cell parameters of the ($P2_1/b$) space group compounds are characterized by the relation $b = 2a$, and therefore, cubic simulation boxes were built as 2 × 1 × 3 or 4 × 2 × 6 supercells, forming a box with a total number of 504 (528 for HOAp) or 4032 (4224 for HOAp) atoms (3D rotatable images in *xyz* format are available for monoclinic hydroxy- and chlorapatite 2 × 1 × 3 supercells). Figure 1 shows a hydroxyapatite 2 × 1 × 3 supercell.

Potential cutoff radii of 8 and 12 Å were used for the 2 × 1 × 3 and 4 × 2 × 6 supercells, respectively. Molecular dynamics simulations were performed using the DL_POLY package[20] and a time step of $t = 1$ fs. The evolution of the systems was monitored during a total time of $t = 200$ ps, and sampling of the appropriate quantities took place after an initial relaxation period, typically 40−60 ps. The Verlet algorithm[21,22] was used to integrate the equations of motion; the Ewald summation method[22,23] was employed to calculate the long-range electrostatic interactions; and the Nosé−Hoover anisotropic thermostat−barostat[23,24] was used to control the temperature and/or pressure. The Ewald method was employed with automatic parameter optimization, according to the procedure described in ref 20, with respect to the Ewald convergence parameter (α), the real-space cutoff, and the total number of *k* space vectors. The precision parameter, *f*, defining the convergence between the total Coulombic energy and the Coulombic virial was set to 1×10^{-3} kJ.

The runs were performed using solids at room temperature ($T = 298$ K) and atmospheric pressure ($p = 1$ bar) to calculate the standard molar lattice enthalpy. To study the solids under high-temperature and/or high-pressure conditions, simulation runs were performed in the ranges 298−1298 K and 0.5−75 kbar, respectively.

TABLE 2: Crystallographic Data at Room Temperature (T = 298 K) and Atmospheric Pressure (p = 1 bar) for Monoclinic ($P2_1/b$) Apatites[a]

	$Ca_{10}(PO_4)_6X_2$											
X	a_{sim}	a_{exp}	δ (%)	b_{sim}	b_{exp}	δ (%)	c_{sim}	c_{exp}	δ (%)	$V_{m.sim}$	$V_{m.exp}$	δ (%)
					2 × 1 × 3 Simulation Box							
OH	9.395	9.421	(−0.3)	18.945	18.843	(+0.5)	6.770	6.881	(−1.6)	525.2	529.0	(−0.7)
Cl	9.500	9.628	(−1.3)	19.220	19.256	(−0.2)	6.719	6.764	(−0.7)	535.2	543.0	(−1.4)
					4 × 2 × 6 Simulation Box							
OH	9.357	9.421	(−0.7)	18.857	18.843	(−0.1)	6.790	6.881	(−1.3)	522.9	529.0	(−1.2)
Cl	9.468	9.628	(−1.7)	19.118	19.256	(−0.7)	6.755	6.764	(−0.1)	533.6	543.0	(−1.7)

[a] The experimental cell angles are as follows: $\alpha = \beta = 90°$ and $\gamma = 120°$. The cell parameters are in Å and molar volumes are in Å·mol^{-1}. Experimental data for HOAp is from ref 4, and that for ClAp is from ref 3.

3. Results and Discussion

Room Temperature and Atmospheric Pressure Simulations: Structural Data. The solid structure integrity of both hydroxy- and chlorapatite was maintained during the entire simulation runs, under the various ensemble conditions: microcanonical (NVE), canonical (NVT), and isothermal−isobaric (NPT). An anisotropic version of the isothermal−isobaric ensemble (NPT),[20] designated as (NσT), was also employed in the simulations. For the NσT ensemble, room temperature (T = 298 K) and atmospheric pressure (p = 1 bar) results are summarized in Table 2.

Deviations of the unit cell lengths and molar volumes from experimental data have a maximum value of ca. 2%, although in most cases the deviations are smaller. The accuracy of the simulated lattice angles is very good, the agreement between calculated and experimental values being within 1% and, for most cases, well below this value. There is no indication of finite size effects, for the results remain pretty much the same when the simulation box size is increased from 2 × 1 × 3 to 4 × 2 × 6.

In Calcium Apatites-I, it was pointed out that the molar volume of hexagonal HOAp obtained in the MD runs, at room temperature and atmospheric pressure, was somewhat higher than the experimental value, and this was attributed to the inability of the dispersive energy parameter, $C_{O(P)-H}$, to deal with the van der Waals energies of the hexagonal phase. As can be seen from Table 2, no such problem arises for the monoclinic polymorph of HOAp; its molar volume is correctly predicted, within ca. 1% from the experimental volume. This is not surprising, since Hauptmann et al.[16] fitted their potential energy parameters to monoclinic crystal data. The model thus accounts for the characteristic interactions between monoclinic O(P) and H, which should be different when considering the same atoms located in a hexagonal lattice, where all the OH^- are oriented along the same direction.

In the next section, results obtained with large (4 × 2 × 6) and small (2 × 1 × 3) supercells are presented. In the subsequent sections, all simulation data will be derived from small supercells and evaluated with a potential cutoff distance of 8 Å and a time step of t = 1 fs.

Room Temperature and Atmospheric Pressure Simulations: Standard Molar Lattice Enthalpy. The calculation of the standard molar lattice enthalpy of a crystalline solid, $\Delta_{lat}H^\circ_{298}$, was already defined in Calcium Apatites-I, along with the relevant thermodynamic equation that allows its calculation from MD data, eq 2.

$$\Delta_{lat}H^\circ_{298} = \Delta_{lat}U^\circ_{298} + 18RT \qquad (2)$$

The generalized Kapustinskii equation proposed by Glasser et al.[25] and Flora et al.[26] will not be considered here due to its inability to distinguish polymorphic compounds. The results obtained in the MD runs are recorded in Table 3, together with the experimental values[1,12] obtained for the hexagonal compounds. From Table 3, it can be seen that the molecular simulations reproduce the experimental lattice enthalpy well, with a deviation less than 1%, for both small (2 × 1 × 3) and large (4 × 2 × 6) simulation boxes.

TABLE 3: Lattice Enthalpies of the Apatites at T = 298 K and p = 1 bar

	$\Delta_{lat}H^\circ_{298}$ [$Ca_{10}(PO_4)_6X_2$] (kJ·mol^{-1})						
X	exp[a] ($P6_3/m$)	sim[b] ($P2_1/b$)	δ (%)	sim[c] ($P2_1/b$)	δ (%)	sim[d] ($P6_3/m$)	δ[e] (%)
OH	34 183 ± 134	34 484	(+0.9)	34 437	(+0.7)	34 004	(+1.4)
Cl	33 836 ± 156	34 042	(+0.6)	33 870	(+0.1)	33 309	(+2.2)

[a] Experimental values for hexagonal apatites.[1,12] [b] Calculated from eq 2 using MD simulation runs with 4 × 2 × 6 supercells. [c] Calculated from eq 2 using MD simulation runs with 2 × 1 × 3 supercells. [d] Calculated from eq 2 using MD simulation runs with 4 × 4 × 6 hexagonal ($P6_3/m$) simulation boxes.[1] [e] Comparison between monoclinic and hexagonal MD results using larger supercells (columns 3 and 7).

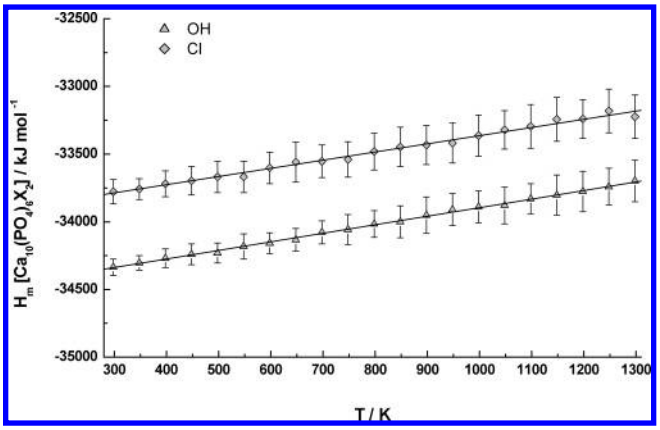

Figure 2. Correlation plots of the molar enthalpy as a function of temperature (p = 1 bar).

In general, the lattice enthalpies calculated using monoclinic crystals present small positive differences from the hexagonal polymorphs, either obtained experimentally or calculated through MD simulations.

High-Temperature Simulations: Heat Capacity at Constant Pressure and Isobaric Thermal Expansivity. The thermal properties of monoclinic hydroxy- and chlorapatite were investigated performing MD runs at atmospheric pressure (p = 1 bar) and spanning a temperature range of 298−1298 K, in 50 K steps. The increase of the molar enthalpy (H_m) with temperature is recorded in Figure 2. It can be well correlated by a linear function (eq 3), whose slope yields the average heat

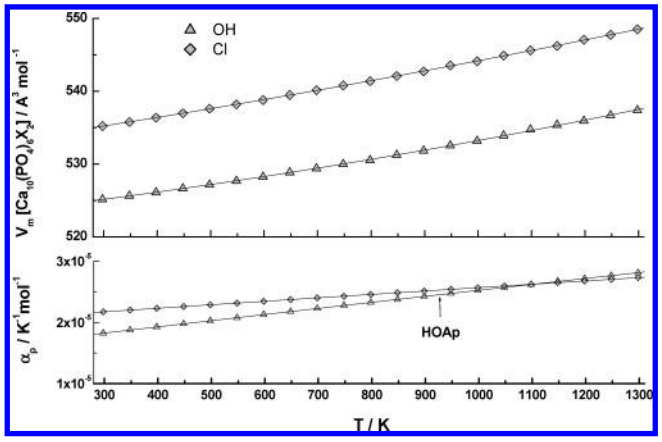

Figure 3. Isobaric lines of volume as a function of temperature at $p = 1$ bar (error bars are smaller than the MD markers) and isobaric thermal expansivity.

capacity at constant pressure, $C_{p,\mathrm{m}}$, in the whole temperature range.

$$H_{\mathrm{m}} = (H_{\mathrm{m},298} - 298C_{p,\mathrm{m}}) + C_{p,\mathrm{m}}T \qquad (3)$$

The parameters and correlation coefficient ($H_{\mathrm{m},298}$, $C_{p,\mathrm{m}}$, R^2) are as follows: (i) HOAp (-34529 ± 6 kJ·mol^{-1}, 635 ± 7 J·mol^{-1}·K^{-1}, 1.00) and (ii) ClAp (-33971 ± 12 kJ·mol^{-1}, 608 ± 14 J·mol^{-1}·K^{-1}, 0.99). The heat capacity at constant pressure of hydroxyapatite agrees, within the standard deviation, with the corresponding quantity previously estimated for the hexagonal polymorph.[1]

It should be noted that the standard deviation of the enthalpy data increases from 0.17% to 0.46% (HOAp) and from 0.26% to 0.48% (ClAp), when the temperature is increased from 298 to 1298K, respectively.

Plotting the molar volume as a function of temperature (Figure 3), one obtains a good representation of the MD data by fitting it to a second-order polynomial. Differentiation of the molar volume with respect to temperature leads to the isobaric thermal expansivity coefficient, $\alpha_p = (1/V_{\mathrm{m}})(\partial V_{\mathrm{m}}/\partial T)_p$. The values of α_p at the two ends of the temperature range are as follows: (i) 1.82×10^{-5} K^{-1}, at $T = 298$ K and 2.81×10^{-5} K^{-1} at $T = 1298$ K for HOAp and (ii) 2.17×10^{-5} K^{-1} at $T = 298$ K and 2.73×10^{-5} K^{-1} at $T = 1298$ K for ClAp.

The dependence of the isobaric expansivity with temperature follows the general trend for solids, that is, it increases with temperature (Figure 3). It is clear from Figure 3 that hydroxy- and chlorapatite exhibit a similar response to temperature. There is a crossover point at T $\approx$ 1100 K. Up to this temperature, the ClAp unit cell expansion is only marginally larger than its hydroxy counterpart, the reverse being the case above that temperature. To probe deeper into the solid structure response to temperature, the individual contributions from the unit cell lengths were separated and normalized through division by their corresponding room temperature values (Figure 4). This procedure clearly shows that the crystal structures of HOAp and ClAp will expand preferentially along the *ab*-crystallographic plane; hydroxyapatite exhibits a slightly greater ability than chlorapatite to deform along the *c*-axis. Since the deformation plot for the *b*-axis is very similar to that for the *a*-axis, it was not represented in Figure 4.

High-Pressure Simulations: Isothermal Compressibility. High-pressure calculations, in the range 0.5−75 kbar, were carried out at room temperature ($T = 298$ K) under the NσT anisotropic isothermal−isobaric ensemble. The behavior of the molar volume as pressure is applied at constant temperature is

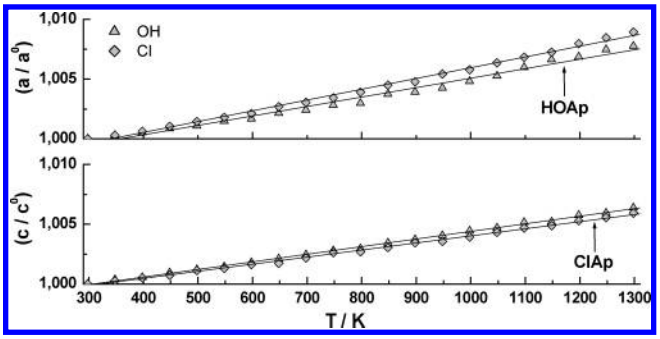

Figure 4. Deformation plots of the normalized unit cell lengths as a function of temperature ($p = 1$ bar). The deformation plot for the *b*-axis is identical to that for the *a*-axis.

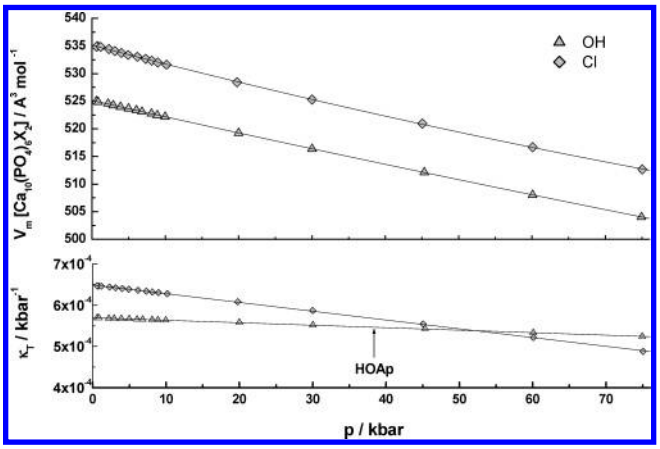

Figure 5. Isothermal lines of volume as a function of pressure at $T = 298$ K (error bars are smaller than the MD markers) and isothermal compressibility.

shown in Figure 5 and indicates that the data are very well described by a second-order polynomial function, similar to what happened in the temperature studies. This functional dependence accounts for the decrease in the isothermal compressibility, $\kappa_T = -(1/V_{\mathrm{m}})(\partial V_{\mathrm{m}}/\partial p)_T$, as pressure is increased, in accordance to what is expected for a solid structure. In the studied pressure range, κ_T appears to vary linearly with pressure, from 5.69×10^{-4} kbar^{-1} ($p = 1$ bar) to 5.24×10^{-4} kbar^{-1} ($p = 75$ kbar) for HOAp and from 6.47×10^{-4} kbar^{-1} ($p = 1$ bar) to 4.88×10^{-4} kbar^{-1} ($p = 75$ kbar) for ClAp.

The isothermal compressibilities of both apatites show the characteristic dependence of a solid phase, namely, a decrease with pressure (Figure 5), reflecting the increasing repulsion of the electronic clouds as applied pressure goes up. The response of both apatites is very similar, but HOAp is marginally less compressible than the chlorinated compound. These findings go in tandem with the high-temperature results obtained in the previous section.

The compression anisotropy exhibited by the hexagonal apatites in Calcium Apatites-I is also present in the monoclinic polymorphs. Both monoclinic hydroxy- and chlorapatite respond to applied pressure by deforming their crystal structure preferentially along a plane defined by the crystallographic *a*- and *b*-axis, as indicated in Figure 6. The deformation plot for the *b*-axis is very similar to the *a*-axis and has been omitted for simplicity sake.

Isothermal Equation of State. In a previous paper, Calcium Apatites-I, we have shown that some widely used equations of state for condensed phases, like the two-parameter Tait EoS[13,27] and the third-order Birch−Murnaghan EoS,[14] do not accurately represent the lower pressure data. The same is true for the

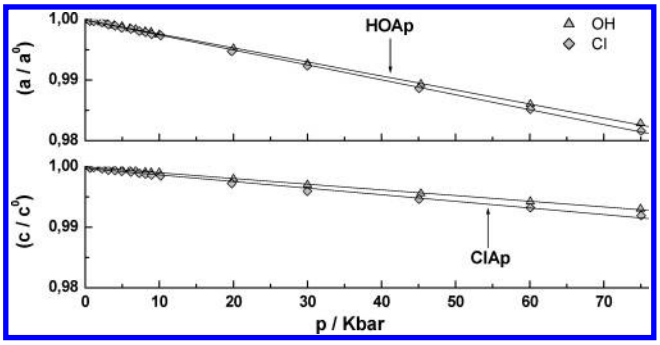

Figure 6. Deformation plots of the normalized unit cell lengths as a function of pressure ($T = 298$ K). The deformation plot for the *b*-axis is identical to that for the *a*-axis.

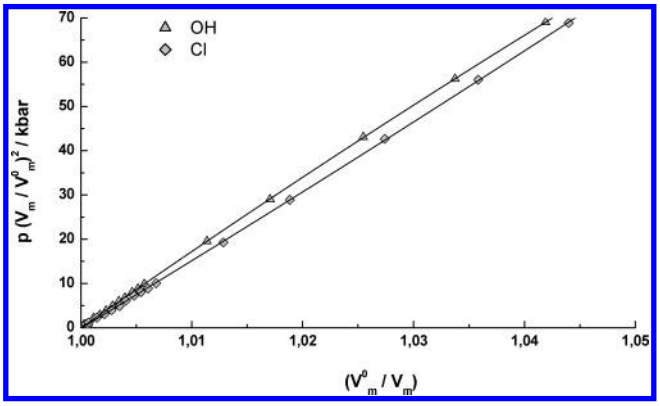

Figure 7. MD results and correlation plots using the PM EoS ($T = 298$ K).

TABLE 4: Parameters of the PM EoS (Equation 4) and Their Correlation Coefficients

	$Ca_{10}(PO4)_6X_2$			
X	A_0 (kbar)	A_1 (kbar)	A_2 (kbar)	R^2
OH	-4.1557×10^3	6.5625×10^3	-2.4066×10^3	1.000
Cl	-2.1325×10^2	-1.0918×10^3	1.3058×10^3	1.000

monoclinic phases. The MD calculations indicate that the more sophisticated Birch−Murnaghan EoS only begins to work at pressures $p > 10$ kbar in the case of HOAp and $p > 20$ kbar for ClAp.

Improving on the work of Vinet and co-workers,[28] Parsafar and Mason[15] derived an equation for a wide variety of substances, including some where phase transitions can occur (PM EoS, eq 4).

$$p\left(\frac{V}{V^0}\right)^2 = A_0 + A_1\left(\frac{V^0}{V}\right) + A_2\left(\frac{V^0}{V}\right)^2 \qquad (4)$$

A_0, A_1, and A_2 are simple functions of the molar volume, bulk modulus, and its pressure derivative, all at zero-pressure. The PM EoS has proven to be extremely useful in describing the high-pressure behavior not only of ionic compounds but also of noble and polar gas solids, metals, and hydrocarbons. We have shown that it can also be successfully applied to hexagonal apatites.[1] Likewise, the full set of data obtained in the present work is well correlated by the second-order polynomial form (on the normalized density, V^0/V) of eq 4, as indicated in Figure 7. The values of the polynomial constants, A_0, A_1, and A_2 and of the corresponding correlation coefficients are recorded in Table 4.

The deviation between the predicted molar volumes and the corresponding MD results is always less than 0.03%, confirming the goodness of the correlation.

4. Conclusions

The agreement obtained between simulated (MD) and experimental structural data is good, the accuracy being better than 2% for ClAp and about 1% for HOAp (Table 2). This validates the rigid model adopted for the phosphate ion in the present work and confirms the findings of Hauptmann et al.[16] in their work with monoclinic HOAp. The model works even under high-pressure conditions. Given the physical nature of the systems (ionic solids of very low compressibility), any contributions of the phosphate modes of vibration to the potential energy should not alter significantly the calculated value.

There are interesting parallels between the high-temperature and high-pressure MD runs in what concerns the deformation of the solid lattice. Starting at room temperature and pressure, ClAp is more susceptible to deformation (expansion with temperature; contraction under pressure) than HOAp, although the difference is small. This seems to indicate that the preferred orientations and interactions of the OH^- ions in adjacent columns appear to stabilize the HOAp monoclinic structure. In the high-temperature ($T > 1100$ K) and high-pressure ($p > 53$ kbar) regions, an inversion occurs and leads hydroxyapatite to become more able to deformation. For monoclinic apatites, isobaric thermal expansion and isothermal compression are anisotropic processes, and we found that the crystal lattice will always deform preferentially along a direction on the crystallographic *ab*-plane.

The full set of high-pressure $p-V_m$ data are very well fitted by the PM EoS, up to 75 kbar. The simulation results and calculated values agree within 0.03%.

Acknowledgment. F.J.A.L.C. gratefully acknowledges a Ph.D. grant from *Fundação para a Ciência e a Tecnologia* (FCT/SFRH/3077/2000).

Supporting Information Available: Crystallographic information files. This information is available free of charge via the Internet at http://pubs.acs.org.

References and Notes

(1) Cruz, F. J. A. L.; Canongia Lopes, J. N.; Minas da Piedade, M. E.; Calado, J. C. G. *J. Phys. Chem. B* **2005**, *109* (51), 24473−24479.
(2) Elliott, J. C. *Structure and Chemistry of the Apatites and Other Calcium Orthophosphates*; Elsevier: Amsterdam, 1994.
(3) Mackie, P. E.; Elliott, J. C.; Young, R. A. *Acta Crystallogr. B* **1972**, *B28*, 1840.
(4) Elliott, J. C.; Mackie, P. E.; Young, R. A. *Science* **1973**, *180*, 1055.
(5) Ikoma, T.; Yamazaki, A.; Nakamura, S.; Akao, M. *J. Solid State Chem.* **1999**, *144*, 272.
(6) Suda, H.; Yashima, M.; Kakihana, M.; Yoshimura, M. *J. Phys. Chem.* **1995**, *99*, 6752.
(7) Takahashi, H.; Yashima, M.; Kakihana, M.; Yoshimura, M. *Thermochim. Acta* **2001**, *371*, 53.
(8) Prener, J. S. *J. Electrochem. Soc.* **1967**, *114*, 77.
(9) Hochrein, O.; Kniep, R.; Zahn, D. *Chem. Mater.* **2005**, *17*, 1978.
(10) de Leeuw, N. H. *Chem. Commun.* **2001**, *17*, 1646.
(11) Born, M.; Huang, K. *Dynamical Theory of Crystal Lattices*; Oxford University Press: Oxford, 1988.
(12) Cruz, F. J. A. L.; Minas da Piedade, M. E.; Calado J. C. G. *J. Chem. Thermodyn.* **2005**, *37*, 1061.
(13) Couchman, P. R.; Reynolds, C. L. *J. Appl. Phys.* **1976**, *47*, 5201.
(14) Angel, R. J. *Rev. Mineral. Geochem.* **2000**, *41*, 35.
(15) Parsafar, G.; Mason, E. A. *Phys. Rev. B* **1994**, *49*, 3049.
(16) Hauptmann, S.; Dufner, H.; Brickmann, J.; Kast, S.; Berry, R. S. *Phys. Chem. Chem. Phys.* **2003**, *5*, 3049.
(17) Tosi, M. P.; Fumi, F. G. *J. Phys. Chem. Solids* **1964**, *25*, 31. Tosi, M. P.; Fumi, F. G. *J. Phys. Chem. Solids* **1964**, *25*, 45.
(18) Mayer, J. E. *J. Chem. Phys.* **1933**, *1*, 270.
(19) Hahn, T., Ed. *International Tables for Crystallography*; Reidel Publishing Company: Dordrecht, The Netherlands, 1983.

(20) Smith, W.; Forrester, T. R. *The DL_POLY package of molecular simulation routines*, version 2.12; The Council for the Central Laboratory of Research Councils: Daresbury Laboratory, Warrington, UK, 1999.
(21) Verlet, L. *Phys. Rev.* **1967**, *159*, 98.
(22) van Gunsteren, W. F.; Berendsen, H. J. C. *Angew. Chem., Int. Ed. Engl.* **1990**, *29*, 992.
(23) Woodcock, L. V.; Singer, K. *Trans. Faraday Soc.* **1971**, *67*, 12.
(24) Nosé, S. *J. Chem. Phys.* **1984**, *81*, 511.
(25) Glasser, L.; Jenkins, H. D. B. *J. Am. Chem. Soc.* **2000**, *122*, 632.
(26) Flora, N. J.; Yoder, C. H.; Jenkins, H. D. B. *Inorg. Chem.* **2004**, *43*, 2340.
(27) Rowlinson, J. S.; Swinton, F. L. *Liquids and Liquid Mixtures*; Butterworth: London, 1982.
(28) Vinet, P.; Ferrante, J.; Smith, J. R.; Rose, J. H. *J. Phys. C* **1986**, *19*, L467.